TIME-DEPENDENT BEHAVIOUR OF THE RECIRCULATION REGION BEHIND AN AXISYMMETRIC BLUFF BODY

V. Gentile, F. F. J. Schrijer, B. W. Van Oudheusden, F. Scarano
Department of Aerodynamics
Delft University of Technology
Kluyverweg 2, Delft, 2629HT, The Netherlands
V.Gentile@tudelft.nl

ABSTRACT

The temporal behaviour of the recirculation region behind an axisymmetric body was characterized at $Re_D = 6.7 \cdot 10^4$ with time-resolved stereoscopic particle image velocimetry (PIV). Measurements were performed at different stations behind the model in planes perpendicular to the freestream flow. Inspection of individual PIV snapshots shows substantial radial offset and irregular azimuthal positioning of the instantaneous backflow region. The time-evolution of the backflow centroid position reveals the transit over the full circumference as a very slow process that takes place at characteristic time-scales in the order of $10^3 \div 10^4$ D/U_∞. The annular shape of the two-dimensional probability distributions of the centroid position indicates that the instability of the axisymmetric wake flow pattern consists of a precession motion about the model symmetry axis.

Proper Orthogonal Decomposition of the fluctuating velocity shows that at all streamwise positions the most energetic dynamics are represented by an asymmetric mode of azimuthal wave-number $m = 1$. Analysis of the corresponding time-coefficients indicates that close to the model this mode is particularly active in the very-low frequency regime, corresponding to $St_D \sim 10^{-4} \div 10^{-3}$, which fact is consistent with the observed slow backflow precession motion. Further downstream the spectral content focuses around a higher and distinct frequency, $St_D \approx 0.25$, which is associated to the large-scale shedding behaviour of the wake.

INTRODUCTION

The wake flow of bluff bodies is characterized by large-scale flow separation, which may introduce unsteady loads. Insight into the flow dynamics of the base region is required in order to understand the origin of these loads.

Previous experiments on the wake of a truncated cylinder at low-speed conditions show that the presence of the recirculation region is associated with strong pressure fluctuations at the base (Merz et al., 1978). Further studies of axi-symmetric wake configurations (Fuchs et al., 1979; Dépres et al., 2004) revealed that the most intense fluctuations are associated with an anti-symmetric vortex-shedding mode (with azimuthal wave-number $m = 1$) occurring at a diameter-based Strouhal number of $St_D \approx 0.2$.

Based on the analysis of base-pressure measurements, Rigas et al. (2014) found evidence that close to the model the anti-symmetric $m = 1$ mode evolves at a very low non-dimensional frequency of $St_D \approx 0.002$. This slow evolution consists of a precession of the stagnation region around the model symmetry axis and reflects an azimuthal shift of the recirculation bubble. As a consequence, axi-symmetry of the wake is obtained only on a long time-averaged basis. A similar symmetry-breaking has been observed to affect the wake behind spheres (Grandemange et al., 2014) and the backflow region in annular jets (Vanierschot and Van Den Bulck, 2014).

The orientation of the vortex shedding on relatively short timescales ($t^* \sim D/U_\infty$) is found to be highly sensitive to the presence of external perturbations (Grandemange et al., 2012), which is confirmed by a number of studies reporting lack of axial symmetry of the wake flow at both subsonic and supersonic conditions (Wolf et al., 2012; Bourdon and Dutton, 1999). While previous authors (e.g. Klei, 2012) claim a careful alignment of the model with respect to the incoming flow as being crucial for wind-tunnel measurements involving blunt-based objects, the presence of a very low frequency instability of the backflow region is now acknowledged as a further aspect to be taken into account, by allowing for a sufficiently long observation-time in order to achieve a converged statistical description of the flow.

While the low-frequency motion of the recirculating flow and its impact on the instantaneous and mean wake topology have been realized, the correlation between the precession motion and the shedding phenomenon still needs further clarification. Moreover the streamwise evolution of the backflow region dynamics has not been characterized yet, since the previous studies mainly have dealt with either pressure measurements at the base (Rigas et al., 2014) or velocity measurements in the reattachment region (Grandemange et al., 2014).

In this respect, the current study aims at a more complete characterization of the time-dependent behaviour of the axi-symmetric wake. For this purpose wind tunnel experiments have been conducted in the near-wake of an ogive-cylinder geometry by means of time-resolved stereoscopic Particle Image Velocimetry (PIV). The measurements were conducted at different distances downstream of the model, in cross-flow planes oriented

perpendicular to the freestream flow. Data were recorded at two different repetition rates, so as to capture both the long-term recirculation instability and the shorter time scale events associated with the shear layer dynamics. The instantaneous velocity field in the near-wake flow is examined by inspecting time-uncorrelated PIV snapshots. Proper Orthogonal Decomposition is used in order to identify the most energetic modes and their characteristic time-scales.

EXPERIMENTAL APPARATUS AND TECHNIQUE

Flow facility and wind-tunnel model

The experiments have been conducted in an open-exit low-speed wind tunnel at the Aerodynamics Laboratories of Delft University of Technology. The model is an ogive-cylinder with 50 mm base diameter and 250 mm length (Figure 1).

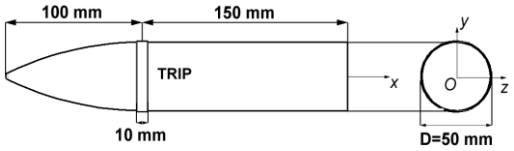

Figure 1. Model schematic: side and back view with coordinate system.

The boundary layer over the model is tripped by means of a 10 mm wide roughness strip of 0.8 mm mean diameter carborundum particles placed at the junction between nose and main body. The mounting of the model allows for translation in the streamwise direction and a fine adjustment of pitch and yaw angles with a precision up to 0.1 degrees, in view of the reported base flow sensitivity towards angular misalignments (Klei, 2012). The model is enclosed in a 40×40 cm^2 transparent test section enabling optical access for illumination. The experiments were performed at a freestream velocity $U_\infty = 20$ m/s, corresponding to a Reynolds number $Re_D = 6.7 \cdot 10^4$ based on the model diameter. The boundary layer at 5 mm upstream of the separation point was measured to have a thickness of $\delta_{95} = 4.5$ mm and $Re_\theta = 900$ (further details can be found in Gentile et al., 2015).

The velocity field in the near-wake of the body was measured with stereoscopic PIV in planes oriented perpendicular to the model axis at positions $x/D = \{0.375, 0.75, 1.125, 1.50\}$ downstream of the model. The location of the measurement planes was chosen such as to span the whole separated region up to the time-averaged reattachment point, which for this configuration is located at $x/D = 1.2$ (Gentile et al., 2015). For each measurement plane 5000 double-frame images are acquired at a repetition rate of either 100 Hz and 2 kHz an acquisition time interval of 50 s and 2.5 s, respectively, or 20,000 and 1,000 in non-dimensional time units (D/U_∞).

Measurement apparatus and procedure

The flow is seeded with micron-sized droplets by means of a SAFEX smoke generator producing a uniform concentration of approximately 5 particles/mm^3. A Quantronix Darwin Duo Nd-YLF (2×25 mJ / pulse at 1 kHz) laser is used for illumination. The thickness of the laser sheet in the measurement region is 3 mm. The pulse separation is set to 25 μs accounting for a maximum particle displacement in the out-of-plane direction of approximately 0.5 mm. The light scattered by the particle tracers is recorded by two Photron FastCAM SA1.1 CMOS cameras (1024×1024 pixels 5400 fps, 20 μm pixel pitch). The angle between the lines of sight of the two cameras is 35 degrees, yielding a relative error in the out-of-plane component equal to 3 (Prasad, 2000). The cameras are equipped with 105 mm focal length Nikkor objectives with aperture set to $f_\# = 2.8$. The field of view (FOV) covers a region of approximately 80×80 mm^2 ($1.6D \times 1.6D$) centered on the model base. The resulting optical magnification factor is $M = 0.17$. A stereoscopic imaging mapping function (Soloff et al., 1997) based on a third-order polynomial is used. Residual misalignments between left and right images are compensated with a self-calibration procedure based on the disparity between left and right images (Wieneke, 2005). The illumination and recording systems are synchronized with a LaVision High Speed Controller hosted by a PC using Davis 8.1 software.

Data processing

Pre-processing is applied to the raw PIV recordings in order to reduce out-of-focus background light intensity. Light reflections from the model base are reduced by a pixel intensity normalization procedure, whereby the intensity of each pixel is normalized with its average value along the sequence. The background intensity is further reduced by subtracting the minimum intensity of a temporally sliding kernel of 11 images.

The velocity vectors are computed by use of an iterative multi-grid cross-correlation analysis based on window deformation (Scarano and Riethmuller, 2000). The final interrogation window is 24×24 pixels (2.8×2.8 mm^2). The window overlap is set at 75% yielding a vector pitch of 0.7 mm (0.014 D). Spurious vectors are detected using the universal median filter (Westerweel and Scarano, 2005). The confidence in the estimation of the particle displacement is assessed by inspecting the signal-to-noise ratio (SNR). For the current case SNR is on average 4 in the separated wake and 1.5 in the shear layer region. As a result, the measurements are considered suitable for the description of the large-scale wake dynamical behaviour, but insufficient for the analysis of the shear layer fine-scale turbulence.

RESULTS

Flow field statistics

The discussion of the near-wake flow is made in terms of non-dimensional properties (indicated by an asterisk),

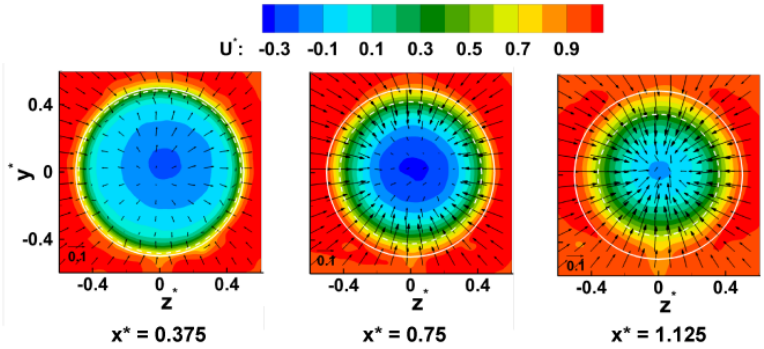

Figure 2. Mean velocity field. Vectors plotted every 7th grid point. Solid line represents the trace of the model base.

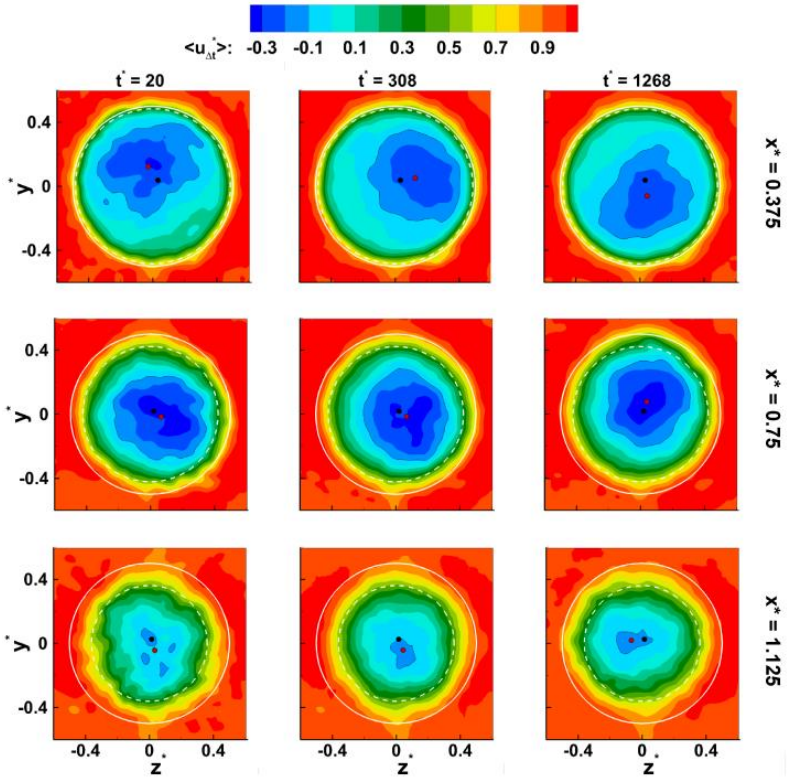

Figure 3. Sliding average of the instantaneous velocity field. Solid line represents the trace of the model base. Dashed line represents the projection of the time-averaged shear layer axis**.**

by scaling dimension with the diameter D, velocities with the freestream velocity U_∞ and time with D/U_∞.

The distribution in the azimuthal plane (z^*, y^*) of the time-averaged velocity are shown in Figure 2, with the colour contours and vectors representing the streamwise and in-plane velocity components, respectively. The time-averaged radial position of the shear layer axis is super-imposed as a dashed line and is obtained from the point of inflection of the velocity profiles in the streamwise symmetry plane $z^* = 0$ (Gentile et al., 2015). The velocity contours define a circular shear layer bounding the wake and an inner region of reverse flow. As the shear layer develops in the streamwise direction, its circumferential axis moves inwards from $x^* = 0.375$, where it is nearly coincident with the trace of the model base, up to the reattachment point where is located at approximately $r^* = 0.39$. This process is accompanied by the shrinking of the inner backflow region. The reverse flow velocity attains a maximum value of 0.31 U_∞ at $x^* = 0.75$. These values are in good agreement with previous studies (Wolf et al., 2012; Wolf, 2013).

Instantaneous velocity field analysis

PIV snapshots of the velocity field data acquired at 100 Hz are inspected in order to examine the features of the instantaneous flow. A sliding-average operation is

applied to the instantaneous measurements, to attenuate the scatter in the data and to emphasize consistent patterns, using a time-interval of $\Delta t^* = 40$ (0.1 s in real time) corresponding to 10 raw snapshots. Series of four of such representations are shown in Figure 3, for $x^* = 0.375$, $x^* = 0.75$ and $x^* = 1.125$. The snapshots span a time-interval of approximately $\Delta t^* = 1600$ (corresponding to 4 s in real time). Additionally, the instantaneous position of the backflow centroid (z^*_c, y^*_c) is super-imposed onto each instantaneous field along with its time-averaged position.

At all streamwise stations evidence is given of a visible radial offset of the instantaneous backflow centroid with respect to its time-averaged position. At $x^* = 0.375$ the separated flow region is approximately circular in shape and its external perimeter is nearly coincident with the trace of the model base. The inner backflow region, on the other hand, displays a significant radial offset. More specifically, the centroid of the backflow region is found to lie typically about 0.1 D off the geometric center of the wake and occupies different azimuthal positions for the realizations shown. The in-plane velocity vectors indicate that the flow surrounding the wake is mostly unperturbed, whereas a radial outwards component is observed in the backflow region. It can be argued that at this distance from the base the inner and outer flow dynamics are uncoupled, the major contribution to the near-wake dynamics being related to the azimuthal motion of the recirculating flow. In particular, the observed radial outwards motion appears to represent a stable condition for the reverse flow streaming towards the base. Given the axial symmetry of the problem such stable condition is independent on the azimuth, which would explain the azimuthal meandering of the backflow region. Further downstream, at $x^* = 0.75$ the wake perimeter appears substantially different from the time-averaged axisymmetric pattern, showing global elongation and displacement from the wake center. The backflow centroid features a much smaller radial offset (~ 0.06 D).

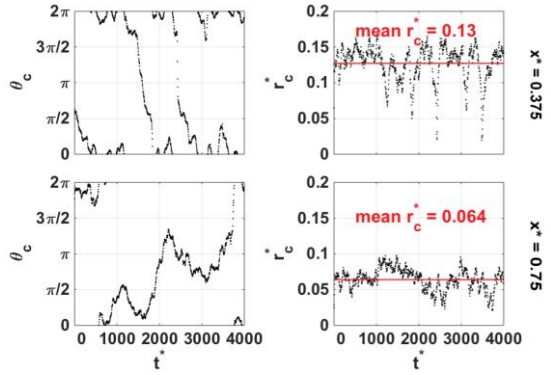

Figure 4. Time-evolution of backflow centroid in the azimuthal and radial direction for different x^*. $\theta_c = (0, 2\pi)$ increasing counter - clockwise starting from $y^* = 0$. Observation-time is $\Delta t^* = 4000$.

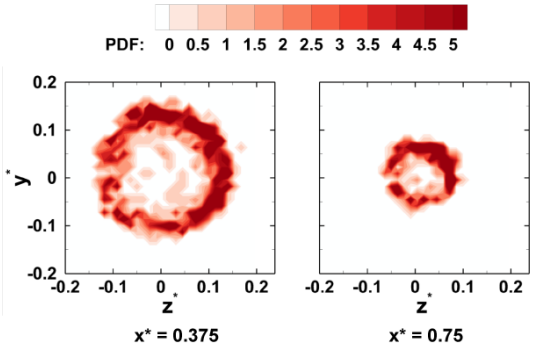

Figure 5. Two-dimensional probability distribution of the backflow centroid position over $\Delta t^* = 2.0 \cdot 10^4$.

The time-evolution of the backflow centroid position presented in Figure 4 reveals the dynamics of the position of the recirculation region over a time interval of 4,000 D/U_∞. At $x^* = 0.375$ the radial position of the centroid oscillates, respectively, between 0.025 D and 0.17 D. The time-evolution of the azimuthal coordinate, on the other hand, suggests the occurrence of preferred positions and that an entire revolution around the wake axis takes on the order of 10^3 D/U_∞ at $x^* = 0.375$ and about four times longer at $x^* = 0.75$.

The annular shape of the two-dimensional probability distribution of the backflow centroid positon shown in Figure 5 indicates that over a sufficiently long time-period (~ 10^4 D/U_∞) the backflow tends to explore all azimuths. A narrow range of most probable radial positions can be identified in the distributions, respectively around $r^*_c = 0.14\ D$ and $r^*_c = 0.08\ D$. This suggests that the backflow motion displays a precession around the model symmetry axis. Previous authors have reported the occurrence of a similar slow precession in axisymmetric turbulent wakes (Rigas et al., 2014; Vanierschot and Van Den Bulck, 2014).

Proper orthogonal decomposition

Snapshot POD (Sirovich, 1987) has been used to identify and characterize the large-scale organization of the flow structures dominating the near-wake dynamics.

The POD energy spectra shown in Figure 6 indicate at all streamwise positions a substantial contribution of the first two POD modes ($k = 1, 2$) to the turbulent kinetic energy, which indicates the occurrence of large-scale fluctuations. The comparative level of the energy content of these modes and their spatial organization (Figure 7) show that they can be interpreted as the orthogonal components of an asymmetric mode of azimuthal wave-number $m = 1$. At $x^* = 0.375$ this mode is particularly strong, capturing about 36% of the fluctuating energy. Its contribution decreases to about 22% moving downstream, where a second mode pair is identified ($k = 3, 4$) and is associated with an $m = 2$ mode. The latter becomes increasingly strong with streamwise distance, capturing up to about 10% of the energy.

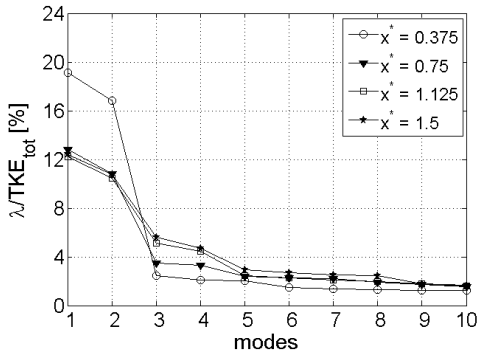

Figure 6. Turbulent kinetic energy distribution over the first 10 modes.

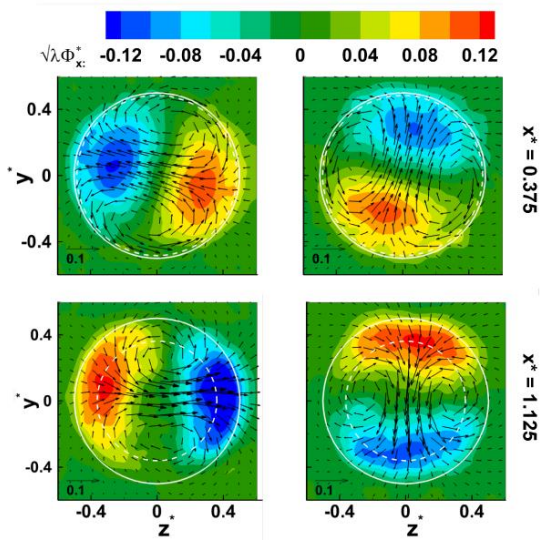

Figure 7. Eigen-functions $k = 1$ (left) and $k = 2$ (right). Vector arrows plotted every 5th grid point represent in-plane components $\sqrt{\lambda}\phi^*_z$ and $\sqrt{\lambda}\phi^*_y$.

The spatial distributions of the $k = 1, 2$ modes shown in Figure 7 outline a dipolar organization, where the linear combination of the two modes allow the reconstruction of a wake offset in any azimuthal direction. The in-plane velocity vectors define two counter-rotating vortices in the azimuthal plane, which can also be recognized in the instantaneous flow realizations (Figure 3). These features have also been observed in the sphere wake by Grandemange et al. (2014), who associated them to the two streamwise vortices arising with the symmetry breaking mode at laminar regime. Close to the model, at $x^* = 0.375$, the peak values of the fluctuations related to this mode are attained in the interior region of the wake, which is in agreement with the backflow region motion inferred from the instantaneous flow realizations. This is consistent also with the interpretation of Rigas et al. (2014), who related the dipolar organization of the first two POD modes of the base pressure fluctuations to the random shift of the base-pressure centroid along the azimuth. Moving downstream to $x^* \geq 0.75$ the modal activity appears to have its peak values along the shear layer, and consequently the dipolar organization is only partly ascribed to the backflow shift, while being increasingly related to the global wake displacement.

Temporal information on the most energetic POD modes are retrieved through analysis of the associated time-coefficients $c_1(t)$ and $c_2(t)$. The frequency spectra of the time-coefficients (see Figure 8) for the first two POD fluctuating modes show that near the model ($x^* = 0.375$) most of the energy is concentrated in the very-low frequency regime, corresponding to $St_D = 10^{-4} \div 10^{-3}$ and is associated with the backflow precession. Moving away from the base this very-low frequency contribution weakens and the energy content tends to shift towards the shedding frequency of $St_D = 0.25$, thus reflecting the growth of large-scale structures in the shear layer.

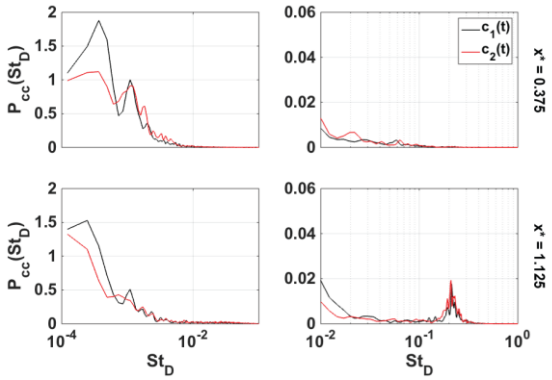

Figure 8. Power spectral density of c_1 and c_2. Sampling frequency is 100 Hz and 2 kHz for the diagrams on the left and right, respectively.

CONCLUSIONS

The temporal behaviour of the recirculation region in the wake of an axisymmetic geometry was characterized by means of time-resolved stereoscopic PIV at a diameter-based Reynolds number $Re_D = 6.7 \cdot 10^4$. Measurements were conducted in different planes oriented perpendicular to the direction of the freestream flow. Velocity data were recorded at low (100 Hz) and high (2 kHz) acquisition frequency, in order to capture both long and short time scale events.

The inspection of time-uncorrelated PIV snapshots obtained at different streamwise stations shows an azimuthal meandering of the recirculation region and a substantial offset with respect to the geometric centre of the distribution. The time-evolution of the centroid position reveals that this process features time-scales in the order of $10^3\, D/U_\infty$. The annular shape of the two-dimensional probability distributions of the backflow centroid position is consistent with the occurrence of a precession motion of the backflow around the model symmetry axis.

The POD modal analysis reveals at all streamwise stations the presence of two dominant modes, which are related to an asymmetric mode of azimuthal wave number $m = 1$. Close to the separation point the activity of this mode is purely associated with the slow backflow precession around the model axis, whereas moving more downstream it is increasingly related to the global wake displacement as a result of large-scale vortex shedding. The power spectra of the time-coefficients confirm that these two processes occur at very different frequency scales, viz. $St_D = 10^4 \div 10^{-3}$ for the slow backflow precession, and $St_D = 0.25$ for the vortex shedding.

REFERENCES

Benedict, L. H., and Gould, L. D., 1996, "Towards better uncertainty estimates for turbulence statistics", *Experiments in Fluids*, Vol. 22, pp. 129-136.

Dépres, D., Reijasse, P., and Dussauge, J. P., 2004, "Analysis of Unsteadiness in Afterbody Transonic Flows", *AIAA Journal*, Vol. 42, pp. 2541-2550.

Fuchs, H. V., Mercker, E., and Michel, U., 1979, "Large-coherent structures in the wake of axi-symmetric bodies", *Journal of Fluid-Mechanics*, Vol. 93, pp. 185-207.

Gentile, V., Schrijer, F. F. J., Van Oudheusden, B. W., and Scarano, F., 2015, *Proceedings, 53rd AIAA Aerospace Sciences Meeting*, AIAA Paper, 2015-1535.

Grandemange, M., Gohlke, M., and Cadot, O., 2014, "Statistical axisymmetry of the turbulent sphere wake", *Experiments in Fluids*, Vol.55, pp. 1-11.

Grandemange, M., Gohlke, M., and Cadot, O., 2012, "On experimental sensitivity analysis of the turbulent wake from an axi-symmetric blunt trailing edge", *Physics of Fluids*, Vol. 24, pp.1-16.

Klei, C. E., "Investigation of the Recirculation Region of a Generic Rocket Configuration Using Stereoscopic PIV", 2012, *Proceedings, 8th Pegasus-AIAA Student Conference*, Poitiers, France.

Merz, R. A., Przirembel, C.E.G., and Page, R. H., 1978, "Subsonic Axi-symmetric Near-wake Studies", *AIAA Journal*, Vol. 16, pp. 656-662.

Prasad, A. K., "Stereoscopic particle image velocimetry", 2000, *Experiments in Fluids*, Vol. 29, No. 2, pp. 103-116.

Rigas, G., Oxlade, A.R., Morgans, A. S., and Morrison, J. F., 2014, "Low-dimensional dynamics of a turbulent axi-symmetric wake", *Journal of Fluid-Mechanics*, Vol. 755, pp. 185-207.

Scarano, F., and Riethmuller, M.L., 2000, "Advances in Iterative Multigrid PIV Image Processing", *Experiments in Fluids*, Vol. 29, pp. 51-60.

Sirovich, L., 1987, "Turbulence and the dynamics of coherent structures. Part 1-3", Quarterly of Applied Mathematics XLV, pp. 561-590.

Soloff, S. M., Adrian, R. J., and Liu, Z. C., 1997, "Distortion compensation for generalized stereoscopic particle image velocimetry", *Measurement Science and Technology*, Vol. 8, pp. 1441-1454.

Vanierschot, M., and Van Den Bulck, E., 2011, "Experimental study of low precessing frequencies in the wake of a turbulent annular jet", *Experiments in Fluids*, Vol.50, pp. 189-200.

Westerweel, J., and Scarano, F., 2005, "Universal Outlier Detection for PIV Data", *Experiments in Fluids*, Vol. 39, pp. 1096-1100.

Wieneke, B., 2005, "Stereo-PIV using self-calibration on particle images", *Experiments in Fluids*, Vol. 39, pp. 267-280.

Wolf, C. C., "The Subsonic Near-Wake of Bluff Bodies", Ph.D. Thesis, Aachen University.

Wolf, C. C., Klei, C. E., Buffo, R. M., Hörnschemeyer, R., and Stumpf, E., 2012, "Comparison of Rocket Near-wakes with and without Nozzle Simulation in Subsonic Freestream Conditions", *Proceedings, 42nd AIAA Fluid Dynamics Conference and Exhibit*, AIAA Paper 2012-3019.